Magalhaes, R.; Duraes, N.; Silva, M.; Silva, J.; Sencadas, V.; Botelho, G.; Gómez Ribelles, JL.... (2011). The role of solvent evaporation in the microstructure of electroactive beta-poly(vinylidene fluoride) membranes obtained by isothermal crystallization. Soft Materials. 9(1):1-14. doi:10.1080/1539445X.2010.525442.

The role of solvent evaporation in the microstructure of electroactive β-poly(vinylidene fluoride) membranes obtained by isothermal crystallization

R. Magalhães[1], N. Durães[2], J. Silva[1,3], M. Silva[1], V. Sencadas[1], G. Botelho[4], J.L. Gómez Ribelles[5,6,7] and S. Lanceros-Méndez[1,*]

[1] *Centro de Física, Universidade do Minho, 4710-057 Braga, Portugal*

[2] *CeNTI - Centre for Nanotechnology and Smart Materials, Rua Fernando Mesquita 2785, 4760-034 Vila Nova de Famalicão, Portugal*

[3] *IPC-Institute for Polymers and Composites, University of Minho, 4800-058, Guimarães, Portugal*

[4]*Departamento de Química, Centro de Química, Universidade do Minho, 4710-057 Braga- Portugal*

[5]*Centro de Biomateriales e Ingeniería Tisular, Universidad Politécnica de Valencia, 46022, Valencia, Spain*

[6]*Regenerative Medicine Unit, Centro de Investigación Príncipe Felipe, Autopista del Saler 16, 46013 Valencia, Spain*

[7] *CIBER en Bioingeniería, Biomateriales y Nanomedicina, Valencia, Spain.*

Abstract

Electroactive β-poly(vinylidene fluoride) membranes were obtained by isothermal crystallization from the solution. Different morphologies and microstructures were obtained by crystallizing at different temperatures. The mechanism and kinetics of solvent evaporation from the polymeric solution were investigated using isothermal thermogravimetric analysis. The kinetic parameters and the activation energy were also

calculated. The solvent evaporation is ruled by two steps, related with a metastable - unstable - metastable transition in the solution phase diagram. Scanning electron microscopy revealed the porous structure and the variations of the morphology with the variation of the isothermal evaporation temperature. Finally, the infrared spectroscopy measurements confirm that the polymer crystallizes in the electroactive β-phase of PVDF.

Keywords: electroactive membranes, PVDF, solvent evaporation, phase diagram

1. Introduction

Poly(vinylidene fluoride), PVDF, is a polymeric material known for its interesting electroactive properties, which allow electro-optical, electro-mechanical and biomedical applications [1, 2].

PVDF is a semicrystalline polymer with uncommon polymorphism among polymeric materials, as it shows at least four crystalline phases called α, β, γ and δ [1, 2]. The one with the best piezo-, pyro-, and ferroelectric properties is the β-phase [1, 2]. Until recently, this phase was exclusively obtained by mechanical stretching of films originally in the non-polar α-phase, which is the most stable one from a thermodynamic point of view when the material is directly obtained from the melt [1, 3]. The stretching process results in films mostly in the β-phase, but with a small amount of the material in the α-phase [3]. Un-oriented films exclusively in the β phase can also be obtained from the crystallization of PVDF from solution with N,N-dimethylformamide (DMF) or dimethylacetamide (DMA) at temperatures below 70 ºC [4, 5]. These films showed a high degree of porosity, which makes them opaque and fragile [6]. This fact opens, on the other hand, the possibility of preparing porous electroactive membranes, with tailored porosity.

The interest in PVDF polymeric membranes is due to its stability against γ-radiation, abrasion and demanding chemical environments, including acids, alkaline, strong oxidants, and halogens. These characteristics make this material suitable for membrane products. PVDF membranes have been investigated using the traditional membrane-

formation methods, such as air-casting of the polymer solution, precipitation from the vapour phase, and thermally induced phase separation [7 - 11].

Some applications have already being explored, in which porous PVDF membranes can play an important role: PVDF has shown high potential to be used as the polymeric matrix for applications on energy storage [12-14].

Magistris *et. al.* [12] showed that, depending on the preparation conditions, PVDF films show different porosity and liquid uptake. The membrane morphology is a relevant parameter which affects the gelation process and the carrier migration properties of the gel electrolytes [12]. It was also concluded that ionic conductivity depends on the amount of liquid electrolyte in the membrane and on the nature of the polymeric matrix [12, 13]. The porous texture also plays an important role in the permeability and conductivity behaviour for applications as polymer electrolyte [12, 13]. A relationship between the membrane performance, the electrochemical property of the electrolyte and the final microstructure was reported by Ji [14].

PVDF porous structures can also find important applications as smart scaffolds with enhanced functionalities [15]. PVDF is a biocompatible polymer and scaffolds of electrospun membranes of this polymer have been reported [15, 16]. Once again, the membrane structure and porosity play an important role in the performance of this material.

Phase separation of the polymer solution for the preparation of porous membranes can be induced by several methods, such as immersion precipitation, air-casting of the polymer solution, precipitation from the vapour phase, and thermally induced phase separation (TIPS) [3,11]. A few works have been reported on preparation of PVDF microporous membrane via TIPS [3, 11, 14, 16, 17]. TIPS has proven to be a valuable method for making commercial membranes. It has several advantages including: a) larger flexibility and easier control than conventional casting processes; b) very low tendency for defect formation; c) very high overall porosity and effective control of the final pore size. In the membrane preparation by the TIPS process, thermodynamic properties, such as the phase diagram can greatly affect the pore size and porosity. The solvents have different effects on the properties of membranes and selecting the proper solvent is one of the key factors for controlling the pore size. For instance, the compatibility of polymer and solvent affects the solution thermodynamic properties such as the binodal line and crystallization temperature. Although different solvents

have effects on membrane morphology, different quenching conditions also affects the polymer crystallization microstructure [9, 10, 18].

The originality of this work is the preparation of PVDF membranes exclusively in the electroactive β-phase of the polymer with controlled porosity by DMF solvent evaporation. Most important, the microstructure of the membranes achieved by solvent evaporation at different isothermal conditions was related to the mechanisms and kinetic parameters of solvent evaporation from the polymeric matrix. In this way, both a method for processing electroactive PVDF membranes and the understanding of the process have been achieved, which ensures reproducibility and further development. The solvent evaporation kinetics was investigated by isothermal thermogravimetric analysis (TGA). The microstructure of the membranes was characterized by scanning electron microscopy (SEM). The spherulite size distribution was also studied and the crystalline polymeric β-phase confirmed in all samples by Fourier transformed infrared spectroscopy (FTIR).

2. Experimental

Poly(vinylidene fluoride) (PVDF) polymer resin (Solef 1010 from *Solvay*) was dissolved in N,N-dimethylformamide (DMF - *Merck*). The initial concentration of solution was 20% (w/w) of PVDF.

After total dissolution of the polymer, isothermal evaporation at different temperatures from 20 to 60 ºC was performed within an air oven (Heraeus). A second method was used, consisting on placing 100 μL of the polymer solution in a pan with a micropipette (*Biohit proline*) and keeping it inside of a thermogravimetric oven at isothermal temperature between 20 to 60 ºC. As the system reached the selected temperature and the value of the sample weight stopped waving, the variation of sample weight over time was registered. All experiments were carried out in a TG1000 from *Rheometric Scientific* under an Argon atmosphere. The microstructure of the membranes obtained by the two different methods was compared by taking scanning electron microscopy (SEM) micrographs with a Leica Cambridge S360 apparatus at room temperature. The phase of the samples was confirmed by Fourier Transformed Infrared Spectroscopy (FTIR) (*Perkin Elmer*, model 1600) in the range between 400 -4000 cm^{-1}.

3. Results

a) Sample morphology and average pore sizes

After polymer dissolution, isothermal evaporation at different temperatures from 20 to 60 ºC was performed in an oven in order to obtain PVDF membranes with different average pore sizes. Figure 1 shows the SEM images of the obtained samples crystallized at room temperature (~20 ºC) and at 30, 40, 50 and 60 ºC.

All samples show a porous structure typical of the β-PVDF crystalline phase [7]. The material crystallized at the lowest temperature presents the highest porosity. The porosity decreases with increasing crystallization temperature, giving origin to higher spherulite radius and smaller porous diameter. The size of the PVDF spherulites was determined by image processing (*Scion image V4.0.3.2*) [19]. The average size of the spherulite diameter is represented in figure 2, demonstrating a linear relationship between spherulite diameter and crystallization temperature.

The differences in the final microstructure found among the samples crystallized at different temperatures is related to the time that the solvent remains in the sample and therefore to the solvent evaporation rate. At high temperatures the solvent is quickly removed given origin to spherulites with higher diameter and small porous radius. At higher crystallization temperatures the polymer chains have enough mobility to occupy the free space left by the solvent. With decreasing crystallization temperature the polymer chains mobility is reduced and seems to be impossible for the polymer to occupy the free space left behind by the evaporated solvent, therefore, the final microstructure show higher porosity and small shperulitic radius. The temperature increase favours polymer diffusion and spherulite growth.
Figure 3 shows the infrared spectra obtained for the sample crystallized at room temperature.

In figure 3 it can be observed that the polymer crystallizes in the β-PVDF crystalline phase. Characteristic absorption bands from the β-phase have been identified at 840,

745, 510, and 445 cm^{-1}. One can also clearly observe the absence of α-phase (408, 532, 614, 764, 796, 855 and 976 cm^{-1}) or γ-PVDF (431, 776, 812 and 833 cm^{-1}) characteristic bands [3, 6]. These results were observed for all samples, showing that if the crystallization temperature is lower than 70 ºC, the polymer crystallizes only in the electroactive β-phase [3, 5, 6].

b) Thermogravimetric analysis

In order to evaluate how the solvent evaporation rate influences the final membrane microstructure, isothermal thermogravimetric analyses were performed at the same isothermal conditions used in the first procedure. After the isothermal experiment, the final microstructure of the samples was also evaluated by SEM in order to corroborate their morphological and phase coincidence to the samples previously presented.

In the thermogravimetric experiments the weight-loss, α, is given by: [20]

$$\alpha = \frac{w_0 - w}{w_0 - w_f} \qquad (1)$$

where *w*, is the weight of the sample and the subscripts *0* and *f* refer to the values at the beginning and end of the weight loss experiment, respectively.

For a single step reaction, the kinetics of the thermal transformation of a solid state chemical reaction is generally described by [20]:

$$r = \frac{d\alpha}{dt} = k(T)\, f(\alpha) \qquad (2)$$

where $f(\alpha)$ is the reaction model, $k(T)$ is the temperature dependent rate constant, T is the temperature, t is the time and r is the degradation rate. The rate constant is normally assumed to obey the Arrhenius equation:

$$k(T) = Z \exp\left(-\frac{E}{RT}\right) \qquad (3)$$

where Z is the pre-exponential factor (sometimes called the frequency factor), E is the activation energy of the kinetic process and R is the gas constant.

If the process is a simple n^{th} order reaction, the conversion dependence can be written as:

$$f(\alpha) = (1-\alpha)^n \quad (4)$$

where *n* is the order of the reaction. Most of the published methods for deriving kinetics parameters from TGA experiments are based in these four equations.
Substituting equation 3 and 4 in equation 2 and taking logarithm, equation 5 is obtained:

$$\ln\left(\frac{d\alpha}{dt}\right) = \ln(Z) + n\ln(1-\alpha) - \frac{E}{RT} \quad (5)$$

In the case of isothermal evaporation, the temperature is constant during the experiment. Therefore, plotting the logarithm of weight-loss rate ln($d\alpha/dt$) vs the logarithm of the percentage of un-evaporated sample ln($1-\alpha$) enables to determine the kinetics order *n* of solvent evaporation, from the slope of this straight line [20].
The weight loss of the PVDF sample during the isothermal experiments was measured for temperatures between 20 and 60 ºC. Figure 4 shows the isothermal TGA traces obtained for the 20% (w/w) PVDF/DMF solution.

After complete solvent evaporation, a weight plateau was reached, corresponding to the mass of the polymer initially present in the solution (20 %). As expected, this plateau is reached more quickly as the isothermal temperature increases, showing that the evaporation of the solvent is faster for higher temperatures. The evolution of the PVDF/DMF weight loss conversion factor (α) is represented in figure 5 for the temperatures used in this work.

Plots of the relative weight loss factor as a function of time showed the sigmoidal shape typical of the isothermal polymer crystallization (Fig. 5). Furthermore, the variation of the initial slope with increasing crystalization temperature indicates a progressively faster crystallization rate: increasing crystallization temperature strongly speeds up the overall crystallization kinetics.

The derivative weight loss curves (figure 6) reveals that the maximum rate of evaporation occurs at the initial steps of the measurements, right before each isothermal temperature is reached, indicating that evaporation is not following a simple *nth* order reaction path. Further, the derivative of the weight loss curves is larger for higher isothermal temperatures, showing the increase of the evaporation rate with increasing temperature.

Figure 6 shows that in all cases, the weight-loss rate ($d\alpha/dt$) as a function of time shows two different steps, which are related to different crystallization acceleration kinetics. It can be observed at the different crystallization temperatures (figure 6) that $d\alpha/dt$ slowly decreases, being this decrease faster with increasing evaporation temperature. As time evolves, an evident transition to a second regime is observed, with $d\alpha/dt$ varying faster with time. Again, the $d\alpha/dt$ variation with time is larger for the higher temperatures (Figure 6).

These results can be understood under the hypothesis that the rate of solvent evaporation from a homogeneous liquid solution is different (slower rate) than the rate of solvent evaporation when polymer crystallization from the solution is taking place (faster rate). Figure 7 shows a schema of the equilibrium phase diagram between the liquid and the crystalline solid of the PVDF-DMF binary system in the temperature range of our experiments, which is far below the equilibrium melting of PVDF (around 170ºC) [21] and far above the equilibrium melting of DMF (-61.2ºC) [22]. Assuming that no liquid-liquid phase separation takes place, an isothermal evaporation process starting with a 20 wt% solution of PVDF in DMF follows a horizontal line that crosses the equilibrium line separating the pure liquid from the solid-liquid biphasic region (solid line in Figure 7). Crystallization nevertheless should start at higher polymer concentration (the dashed line). The situation is analogous to what happens when crystals are formed from a solution that is cooled down keeping the concentration constant. In this case, crystal growth only takes place when stable nuclei are formed. This happens at a temperature that is significantly lower than that of the equilibrium

line. In our isothermal experiment stable nuclei can only be formed when the polymer concentration is higher than that of the equilibrium diagram. At that moment exothermal growth of the crystals accelerates the rate of solvent evaporation as detected in the TGA experiments by a faster rate of weight decrease. Spherulite growth produces a semicrystalline PVDF with amorphous layers between lamellae [1]. The second stage of weight loss shown in Figure 6 follows until just the solvent entrapped in the amorphous PVDF layers remains in the sample. The slow evaporation of this residual solvent is also clearly shown in Figure 6.

The time instant at which crystal growth starts can be determined from Figure 6 for the samples crystallized in the temperature range between 40 and 60ºC (dashed lines). Then, the weight loss for that time allows the calculation of the polymer concentration of the solution in Figure 4. Thus, at 60ºC crystallization starts when the solution contains 77 wt% PVDF, 68 wt% at 50ºC and 61 wt% at 40ºC, as schematized in Figure 7. The results are more uncertain for lower crystallization temperatures.

The morphology of the porous polymer obtained after isothermal crystallization can be interpreted as a result of the temperature dependence of nucleation. As temperature decreases, the critical size of the stable crystallization nucleus decreases, therefore, the probability of the beginning of a spherulite growth increases. In Figure 1 it can be observed that the number of spherulites increases with decreasing temperature. At the lowest crystallization temperature the amount of spherulites growing simultaneously is so high that the polymer of the solution is consumed before the growing spherulites contact each other. Consequently, the final morphology is that of loosely adhered crystal microspheres. At higher temperatures, the SEM picture still allows identifying the individual spherulites. In this case, the spherulites are adhered to each other, leaving as pores the spaces left between the formed crystal microspheres. According to this interpretation the pore size is related to crystal nucleation, being smaller as smaller is the size of the spherulites or larger the number of spherulites growing simultaneously. The phenomenon is similar to that of the spherulitic growth of a pure polymer when the crystals grow consuming the liquid phase. The main difference is that when crystallizing from the solution, the solvent elimination leaves an empty volume that will result in the pore structure of the membrane.

Previously it was shown that the weight-loss rate $d\alpha/dt$ as a function of time was ruled by a two step process. This is related to the system course between the spinodal decomposition (SD) and the nucleation growth (NG) phase separation. The SD process is a spontaneous process unlike the NG mechanism. A transition between the SD and NG will be detectable in the crystallization kinetics explaining the origin of the two step process. For all isothermal temperatures (except in the lowest) there are two transitions: the first from NG to SD and the second from NG to SD.

The slopes of the two steps of weight-loss rate $d\alpha/dt$ are represented in Figure 8 for the different isothermal crystallization temperatures. Figure 8 shows that the two processes follow the same pattern, but the variation with increasing crystallization temperature is larger for the second regime. This result indicates that crystallization kinetics is more pronounced at this later stage.

Importancia de la cuantificación

The plots of $\ln(d\alpha/dt)$ against $\ln(1-\alpha)$ for isothermal evaporation (Figure 9) can be fitted by linear relations and analyzed using the n*th* order method (Pearson R^2 > 92% confidence). In this way, the reaction order n can be obtained ("general rate expression", equation 5).

The reaction order calculated for the PVDF-DMF solution under isothermal conditions at different temperatures is represented in figure 10. The values obtained for the reaction order of the PVDF-DMF evaporation under isothermal conditions varies from 0.07 to 0.3 with increasing temperatures from 20 to 60 ºC.

The determination of the kinetic parameters over a series of weight losses has more accuracy than the method of the "general rate expression". Flynn [23, 24] developed a method to calculate the kinetic parameters at different conversion levels using isothermal techniques:

$$\ln(t) = \ln\big(g(\alpha)\big) - \ln(A) + \frac{E_{act}}{RT} \qquad (6)$$

In equation 6, *t* is time, *g(α)* is constant at α intervals, *A* is a constant, *R* is the ideal gas constant, *T* is the temperature of isothermal measurement and E_{act} is the activation energy.

Equation 6 provides a way of calculating E_{act} if the evaporation mechanism remains unchanged during the isothermal experiment at the α intervals under consideration. This is method is based on the slope of a plot of natural logarithm of time *vs* inverse absolute test temperature, as presented in figure 11.

It can be observed that the data in figure 10 shows good linearity. The linear correlation coefficients obtained by fitting with equation 6 are all higher than 0.99. The slope of these linear fittings (Figure 11) decreases with the increase of weight loss α over the range 30 – 90%, implying a conversion dependency of the activation energy.

The dependence of activation energy as a function of weight loss α, derived from the isothermal experiments, is presented in figure 12.

Conclusions

Electroactive β-PVDF membranes with different spherulite and pore sizes were prepared by DMF solvent evaporation at different isothermal temperatures below 70 ºC. The evaporation mechanism leading to the different microstructures has been studied by TGA. Isothermal crystallization data of PVDF was analyzed using the "general rate expression" and the iso-conversional procedure developed by Flynn. These two techniques show that the reaction order n*th*, determined at each isothermal temperature, varies in the range from 0.07 to 0.3. The activation energy shows a temperature dependency in the weight loss range of 30-90%.

The temperature and consequently the crystallization time have influence on the microstructure of samples. The polymer crystallizes in the β-PVDF crystalline phase.

The spherulite size is higher with increasing the crystallization isothermal temperatures. On the other hand the pore diameter decreases with the increase of the crystallization temperature, which is also related to the initial position of the system in the phase diagram along the temperature axes.

Acknowledgements

The authors thank the Portuguese Foundation for Science and Technology (FCT) Grants PTDC/CTM/73030/2006, PTDC/CTM/69316/2006 and NANO/NMed-SD/0156/2007. V. Sencadas thanks the FCT for the SFRH/BPD/63148/2009 grant. JLGR acknowledge the founding form the Programa de Apoyo a la Investigación y Desarrollo (PAID-00-09) of the Universidad Politécnica de Valencia for a short stay in Universidade do Minho, Braga, the support of the Spanish Ministry of Science through project No. MAT2007-66759-C03-01 (including the FEDER financial support) and funding for research in the field of Regenerative Medicine through the collaboration agreement from the Conselleria de Sanidad (Generalitat Valenciana), and the Instituto de Salud Carlos III (Ministry of Science and Innovation). The authors also thank to *Solvay* for providing the excellent quality material.

References

[1] Lovinger AJ, Developments in Crystalline Polymers, Vol. 1, D.C. Basset, London, Elsevier Applied Science, 1982

[2] Nalwa HS, Ferroelectric Polymers: Chemistry, Physics, and Applications, Vol 1 Marcel Dekker, Inc, New York, 1995

[3] Sencadas V, Gregorio Jr. R, Lanceros-Mendez S, J. Macromol. Sci. Part B Phys. 2009; 48: 514-525.

[4] Gregorio Jr. R, Cestari M, J. Polym. Sci. Part B: Polym. Phys. 1994; 32: 859-870.

[5] Gregorio Jr. R, J. Appl. Polym.r Sci. 2006; 100: 3272-3279.

[6] Sencadas V, Gregorio Filho R, Lanceros-Mendez S. J.Non-Cryst. Solids 2006; 352: 2226–2229.

[7] Matsuyama H, Teramoto M, Nakatani R, Maki T, J. Appl. Polym. Sci. 1999; 74: 159–170

[8] Matsuyama H, Teramoto M, Nakatani R, Maki T. J. Appl. Polym. Sci., 1999; 74: 171–178

[9] Matsuyama H, Teramoto M, Kudari S, Kitamura Y. J. Appl. Polym. Sci.,2001; 82: 169–177

[10] Su Y, Chen C, Li Y, and Li J; J. Macromol. Sci., Part A Pure Appl Chem 2007; 44: 99–104

[11] Han X, Ding H, Wang L, Xiao Ch. J. Appl. Polym. Sci.2008; 107: 2475–2479

[12] Magistris A, Quartarone E, Mustarelli P, Saito Y, Kataoka H, Solid State Ionics 2002; 152-153: 347-354.

[13] Quartarone E, Mustarelli P, Magistris A, J. Phys. Chem. B 2002; 106: 10828-10833.

[14] Ji GL, Zu BK, Cui ZY, Zhang CF, Xu YY, Polymer 2007; 48: 6415-6425.

[15] Sencadas V, Rodriguez JC, Ribeiro C, Gómez Ribelles JL, Lanceros-Méndez S, Mater. Res. Soc. Symp. Proc. 2009; 1140.

[16] Ding Y, Zhang P, Long Z, Jiang Y, Xu F, Di W, Science Technology. Adv. Mater. 2008; 9: 015005-4.

[17] Su Y, Chen CX, Li YG, Li JD, J. Macromol. Sci. A 2007; 44: 99-104.

[18] Yeow ML, Liu YT, Li K; J. Appl. Polym. Sci. 2004; 92: 1782–1789

[19] http://www.scioncorp.com

[20] Charsley EL, Warrington SB. Thermal Analysis-techniques and applications. The Royal Society of Chemistry (1992).

[21] Mark JE, Polymer Data Handbook, Oxford University Press, Oxford, 1999

[22] Smirnova NN, Tsvetkova LYa, Bykova TA and Marcus Y, The Journal of Chemical Thermodynamics, 2007; 39: 1508-1513

[23] J. H. Flynn, Thermal analysis, Academic Press, New York, 1969.

[24] J. H. Flynn, Laboratory Preparations in Molecular Chemistry, MacGrawl-Hill, New York, 1970.

Figure Captions

Figure 1 – SEM surface image of PVDF samples crystallized at different temperatures: **a)** room temperature, **b)** 30ºC, **c)** 40ºC, **d)** 50ºC and **e)** 60ºC.

Figure 2 – Average spherulite size for samples crystallized under isothermal conditions.

Figure 3 – Infrared spectra for the PVDF sample crystallized at room temperature (the arrows mark the absorption bands characteristic of the β-PVDF).

Figure 4 – Weight loss curves of a PVDF-DMF solution at several isothermal temperatures.

Figure 5 – Conversion rate, α at different temperatures for the PVDF/DMF solution.

Figure 6 – Dependence of the weight-loss rate ($d\alpha/dt$) on heating time for the PVDF-DMF solution measured at several isothermal temperatures.

Figure 7 – Phase diagram for the PVDF/DMF solution, the dashed line corresponds to the start of crystal growth while the solid line is the equilibrium one. The arrows represent the system evolution to solvent evaporation.

Figure 8 – Slope of weight-loss rate $d\alpha/dt$ on time for the PVDF-DMF solution measured at several isothermal temperatures. The squares are the slope for the first $d\alpha/dt$ regime and the red dots are the slope for the second regime.

Figure 9 – $\ln(d\alpha/dt)$ against $\ln(1-\alpha)$ plots for isothermal evaporation for the PVDF-DMF solution measured at different temperatures.

Figure 10 – Reaction order obtained by the "general rate expression" for the PVDF-DMF solution under isothermal conditions.

Figure 11 – Flynn method estimation of activation energy for the PVDF/DMF under isothermal conditions.

Figure 12 – Evolution of the activation energy obtained by the Flynn method for different levels of conversion.

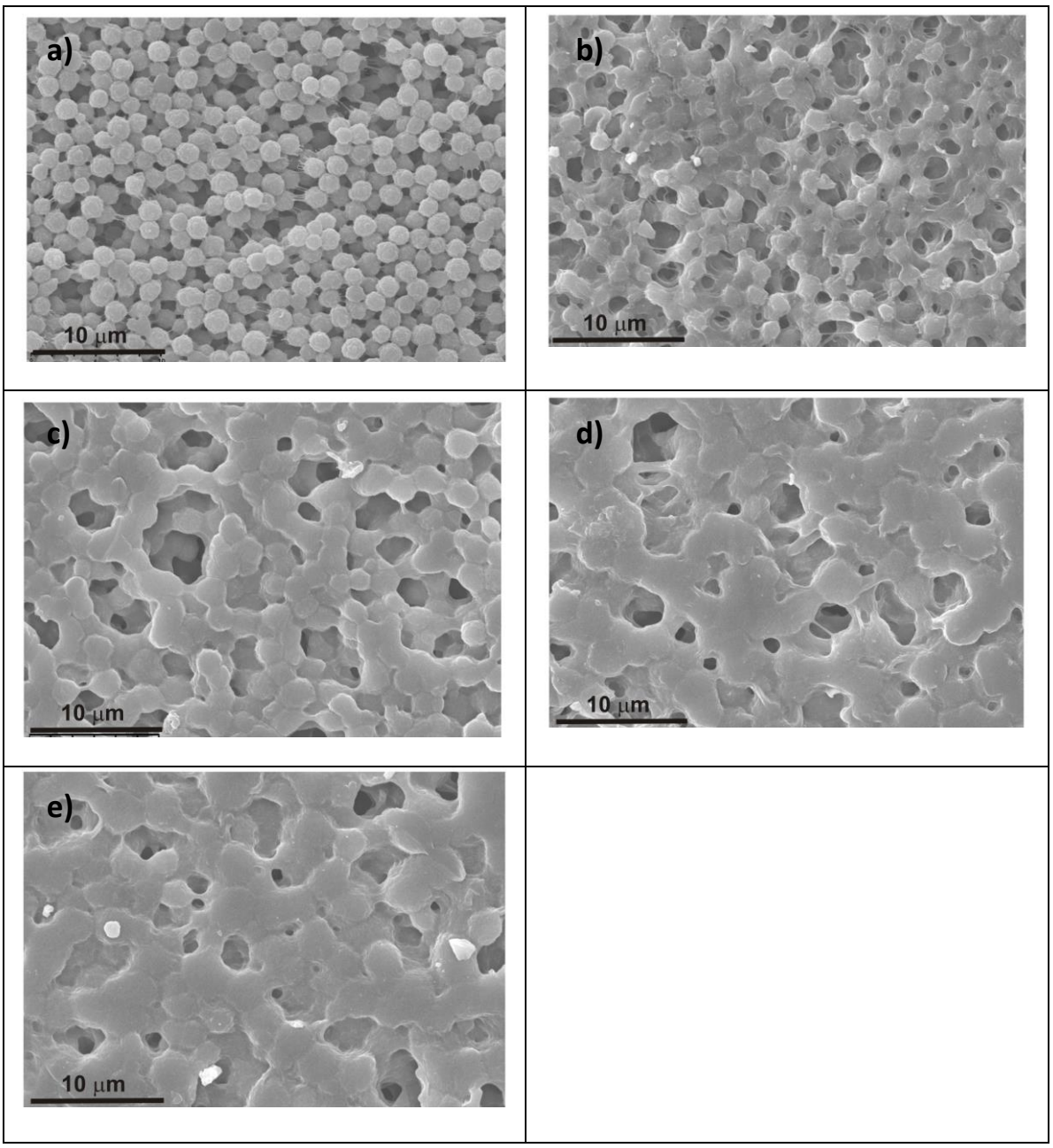

Figure 1 – SEM surface image of PVDF samples crystallized at different temperatures: **a)** room temperature, **b)** 30ºC, **c)** 40ºC, **d)** 50ºC and **e)** 60ºC.

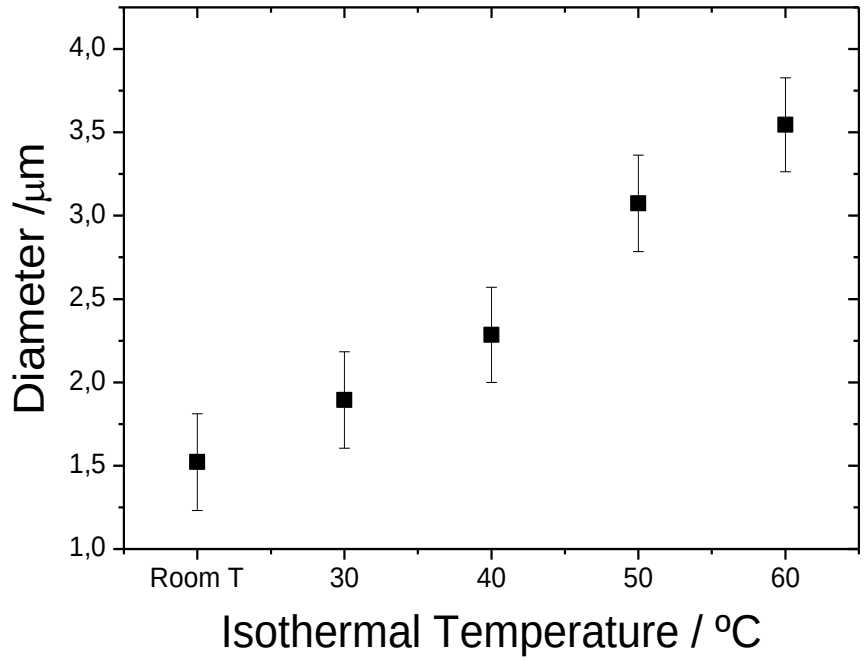

Figure 2 – Average spherulite size for samples crystallized under isothermal conditions.

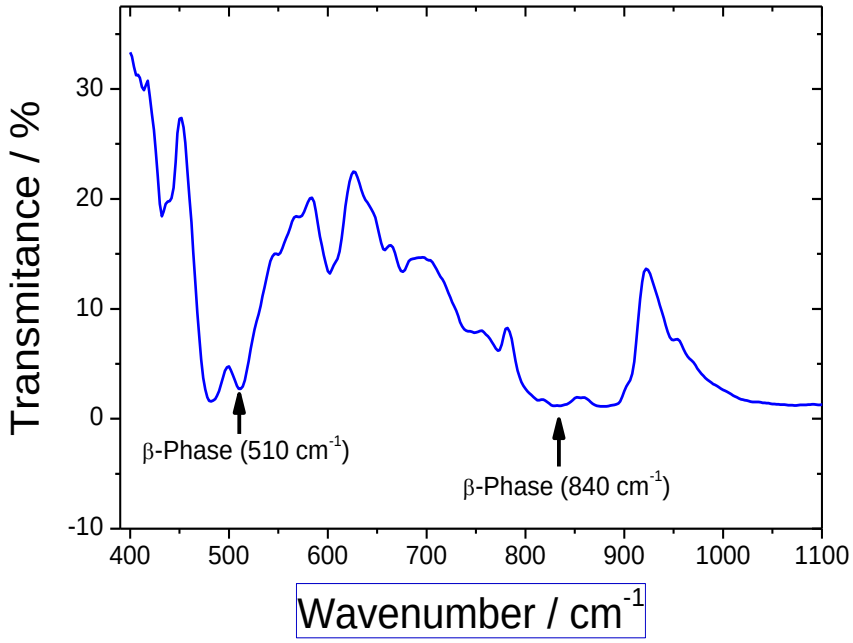

Figure 3 – Infrared spectra for the PVDF sample crystallized at room temperature (the arrows mark the absorption bands characteristic of the β-PVDF).

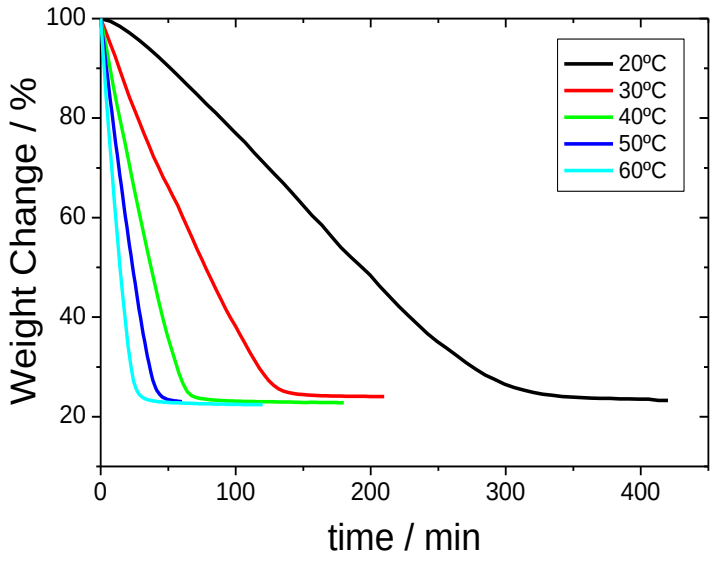

Figure 4 – Weight loss curves of a PVDF-DMF solution at several isothermal temperatures.

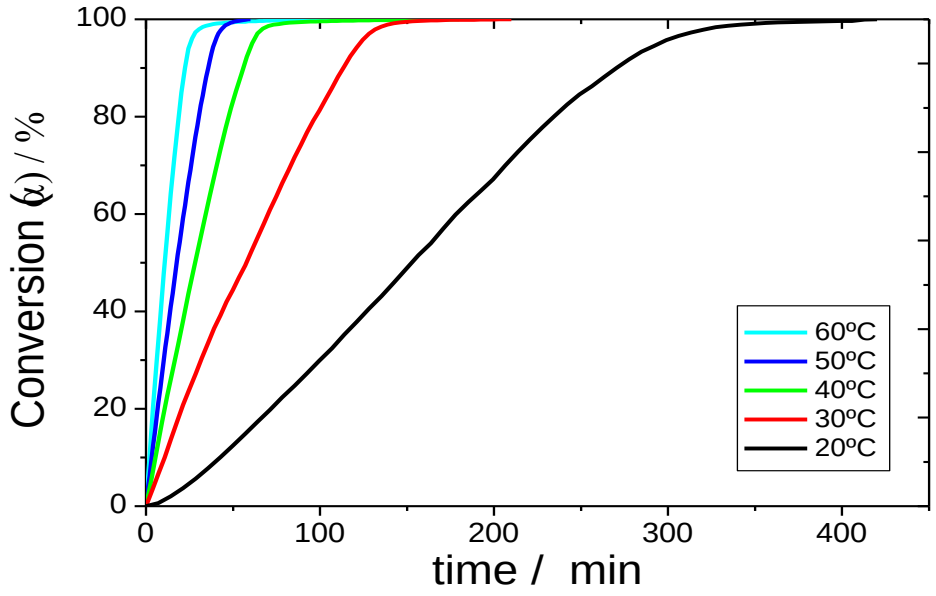

Figure 5 – Conversion rate, α at different temperatures for the PVDF/DMF solution.

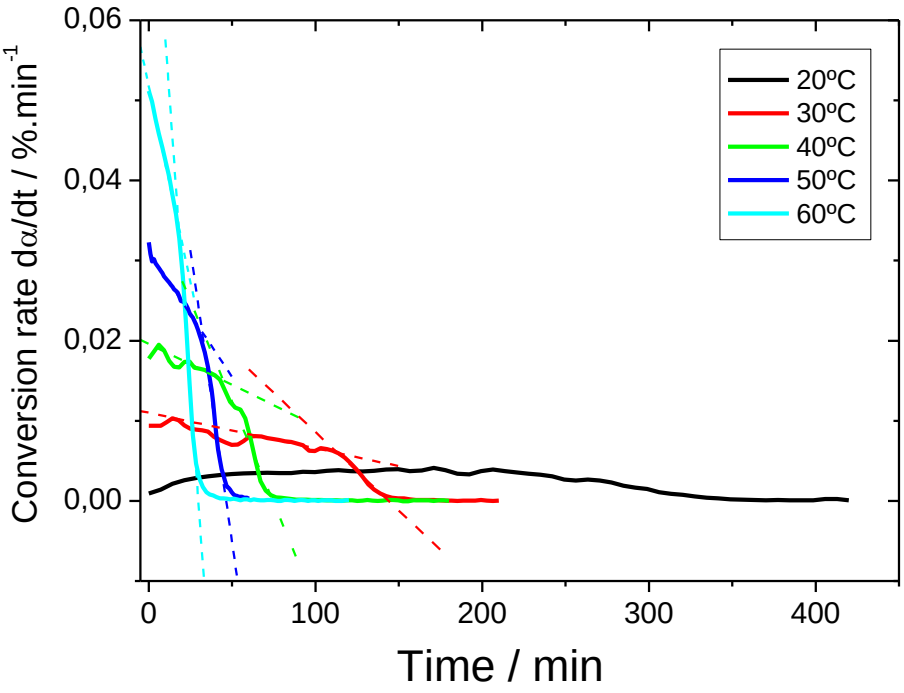

Figure 6 – Dependence of the weight-loss rate (*dα/dt)* on heating time for the PVDF-DMF solution measured at several isothermal temperatures.

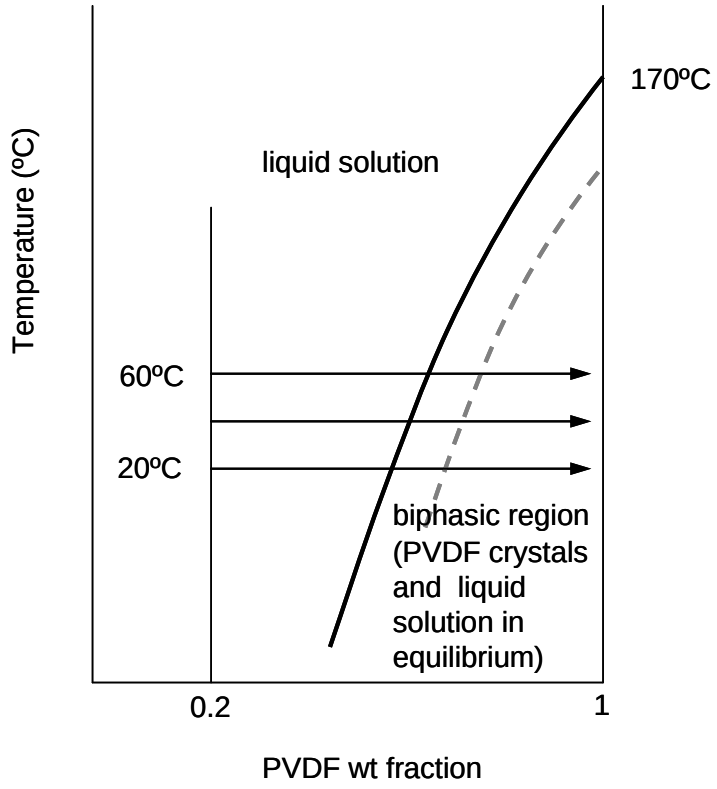

Figure 7 – Phase diagram for the PVDF/DMF solution, the gray dashed line corresponds to the start of crystal growth while the black line is the equilibrium one. The arrows represent the system evolution due to solvent evaporation.

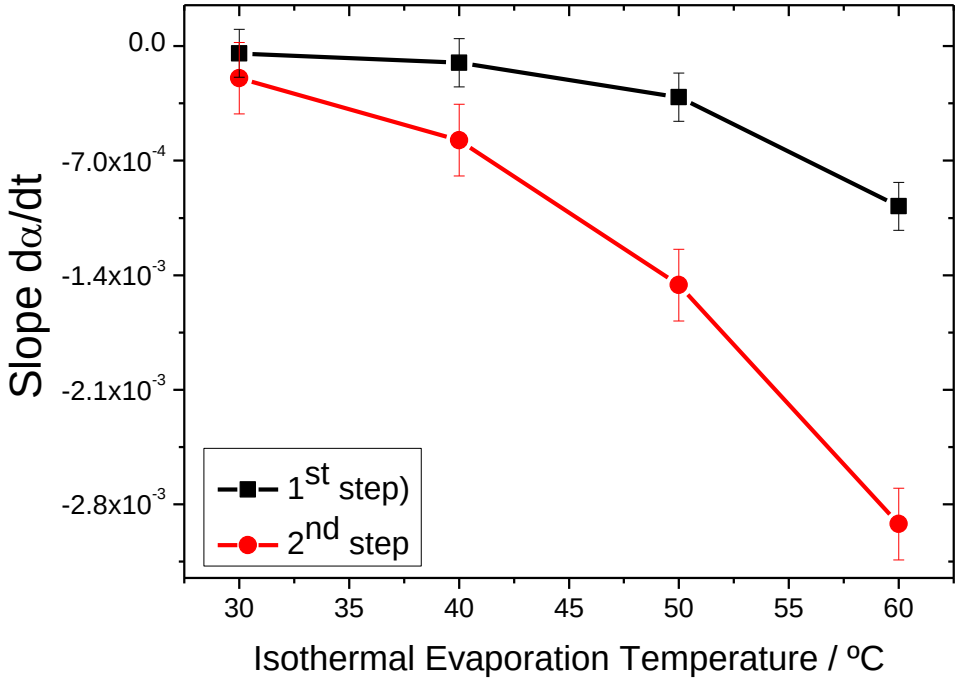

Figure 8 – Slope of weight-loss rate $d\alpha/dt$ on time for the PVDF-DMF solution measured at several isothermal temperatures. The squares are the slope for the first $d\alpha/dt$ regime and the red dots are the slope for the second regime.

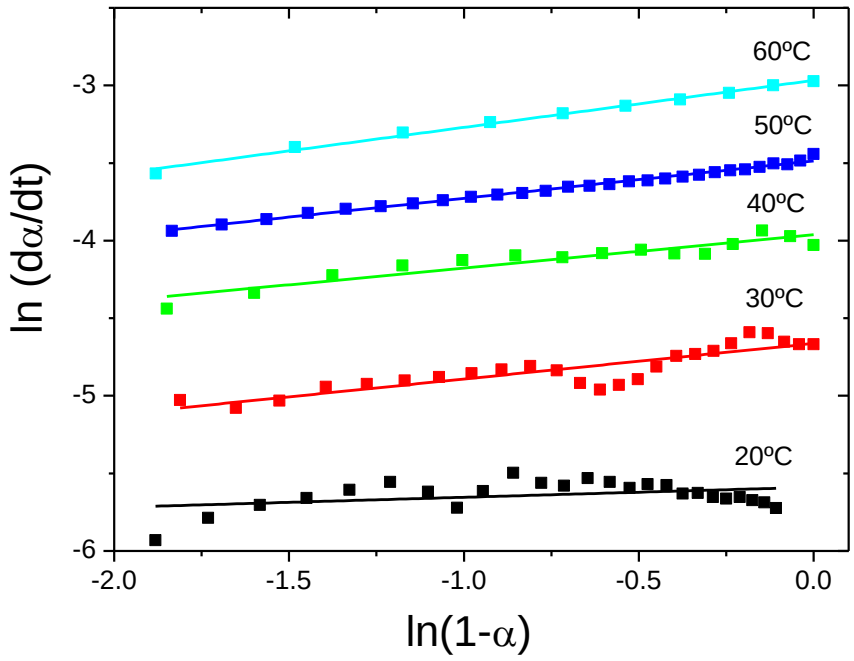

Figure 9 – ln(*dα*/*dt*) against ln(*1*-α) plots for isothermal evaporation for the PVDF-DMF solution measured at different temperatures.

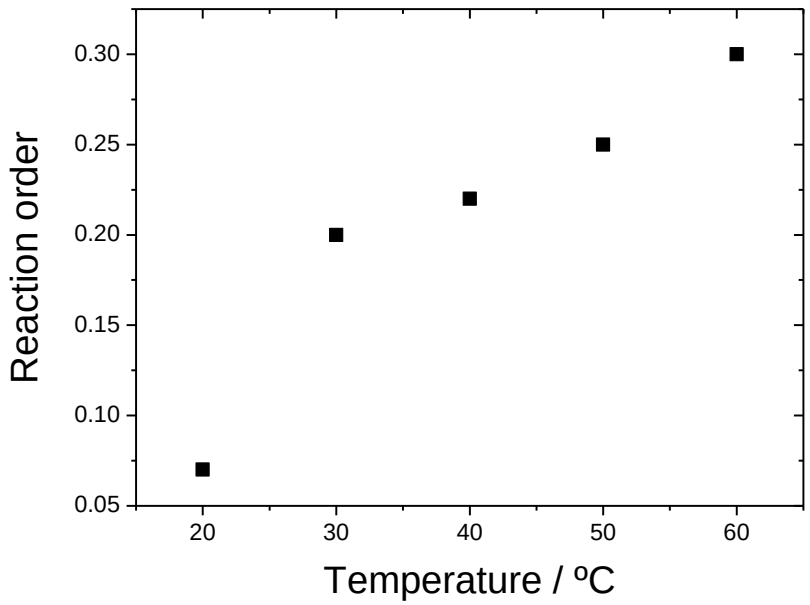

Figure 10 – Reaction order obtained by the "general rate expression" for the PVDF-DMF solution under isothermal conditions.

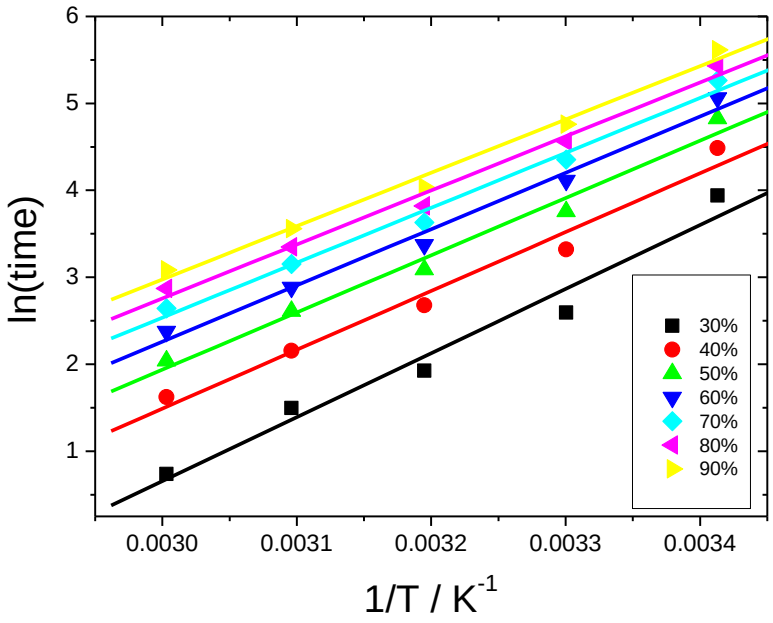

Figure 11 – Flynn method estimation of activation energy for the PVDF/DMF under isothermal conditions.

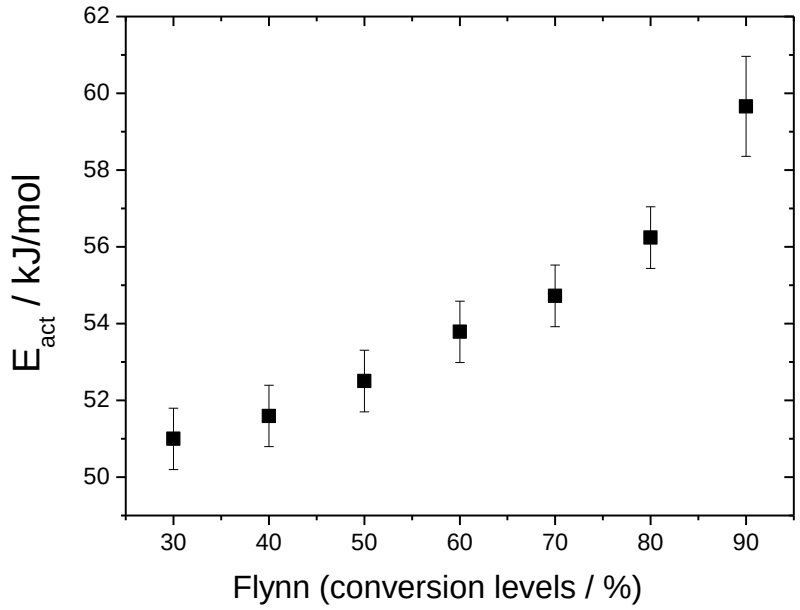

Figure 12 – Evolution of the activation energy obtained by the Flynn method for different levels of conversion.